PERMAFROST AND PERIGLACIAL PROCESSES
Permafrost and Periglac. Process. (2011)
Published online in Wiley Online Library
(wileyonlinelibrary.com) DOI: 10.1002/ppp.709

Biogeochemical and Geocryological Characteristics of Wedge and Thermokarst-Cave Ice in the CRREL Permafrost Tunnel, Alaska

Thomas A. Douglas,[1]* *Daniel Fortier*,[2] *Yuri L. Shur*,[3] *Mikhail Z. Kanevskiy*,[2] *Laodong Guo*,[4] *Yihua Cai*[5] *and Matthew T. Bray*[3]

[1] Cold Regions Research and Engineering Laboratory, Fort Wainwright, Alaska, USA
[2] Institute of Northern Engineering, University of Alaska Fairbanks, Fairbanks, Alaska, USA
[3] Department of Civil and Environmental Engineering, University of Alaska Fairbanks, Fairbanks, Alaska, USA
[4] University of Southern Mississippi Department of Marine Science, Stennis Space Center, Mississippi, USA
[5] Xiamen University College of Oceanography and Environmental Science, Xiamen, Fujian, China

ABSTRACT

Partially eroded ice wedges and lenticularly shaped bodies of massive thermokarst-cave ice in ice-rich syngenetic permafrost (yedoma) are exposed in the CRREL tunnel near Fairbanks, Alaska. The ice wedges, which formed 25 000 – 40 000 years ago, were subsequently affected by localised thermal erosion, resulting in underground cavities that filled with surface water infiltrating through a network of conduits. This water froze inward from the walls of the cavity. We report the biogeochemical characteristics of one of these thermokarst-cave ice features and four nearby ice wedges. The thermokarst-cave ice has 30 times the dissolved organic carbon concentration, 20 times the total dissolved nitrogen concentration and five to 20 times the inorganic solute concentrations of the surrounding (original) ice wedge material. Based on these results we present a schematic model to describe how the thermokarst-cave ice was formed and preserved and what processes led to its current biogeochemical characteristics. Current estimates of soluble solutes stored in permafrost may underestimate the total carbon and nutrient load where wedge material has been extensively replaced by surface water rich in organic carbon, nutrients or inorganic solutes. Published in 2011 by John Wiley & Sons, Ltd. This article is a US Government work and is in the public domain in the USA.

KEY WORDS: permafrost; thermokarst-cave ice; organic carbon storage; Alaska

INTRODUCTION

Between 400 and 450 Gt of carbon are currently estimated to be locked in syngenetically frozen ice-rich silt in the northern hemisphere (Zimov *et al.*, 2006a, 2006b; Tarnocai *et al.*, 2009). Much of this pool of organic carbon has been preserved in permafrost for millennia but it could be liberated if the permafrost thaws (Oechel *et al.*, 1993; Petrone *et al.*, 2006; Bockheim and Hinkel, 2007; Guo *et al.*, 2007) due to climate warming (Shur and Jorgenson, 2007) or localised degradation (e.g. Linnel, 1973; Viereck, 1982; Burn, 1998; Hinzman *et al.*, 2003; Fortier *et al.*, 2007a; Douglas *et al.*, 2008). As a consequence, the biogeochemistry and preservation history of frozen soils, ice wedges and other permafrost features may become highly significant for the future Arctic nutrient cycle.

The Cold Regions Research and Engineering Laboratory (CRREL) Permafrost Tunnel in Alaska provides easy access to frozen ice-rich sediments for mapping, photographic documentation and sample collection. An important but under-investigated feature in the tunnel is thermokarst-cave ice, which forms when thermal erosion creates open cavities in ice wedges and the surrounding soil which subsequently fill with surface water that freezes (Murton and French, 1993). The characteristics of this ice are not well known and even less is understood about its distribution worldwide (Shur *et al.*, 2004). Thermokarst-cave ice has been reported in Canada (French, 1975; Mackay, 1997; Allard and Kasper, 1998) and various locations in Alaska and Siberia (Shumskii, 1959; Gasanov, 1969; Vtyurin, 1964; Rozenbaum *et al.*, 1978; Popov *et al.*, 1985; Fortier *et al.*, 2007b; Kanevskiy *et al.*, 2008).

In this paper we compare the biogeochemical characteristics of a thermokarst-cave ice body with those of four ice

* Correspondence to: Thomas A. Douglas, Cold Regions Research and Engineering Laboratory, PO Box 35170, Fort Wainwright, Alaska 99703-0170, USA. E-mail: thomas.a.douglas@usace.army.mil

Contract/grant sponsors: National Science Foundation Office of Polar Programs; 0454939.

Received 12 January 2010
Revised 16 November 2010
Accepted 16 November 2010

Published in 2011 by John Wiley & Sons, Ltd.

wedges in the CRREL Permafrost Tunnel. We synthesise our results into a schematic model to describe how the thermokarst-cave ice feature was formed and preserved and what processes led to its biogeochemical characteristics. We also provide ways to physically and chemically identify this ice in the permafrost record and how to distinguish it from ice wedges.

PERMAFROST WITHIN THE CRREL PERMAFROST TUNNEL IN INTERIOR ALASKA

The CRREL Permafrost Tunnel is located in Interior Alaska (64.952°N, 147.617°W) in a gently sloping northwestward-facing hill 11 km north of Fairbanks. The tunnel was excavated in the 1960 s through Late Pleistocene-age aeolian silt (loess), reworked loess and alluvium that comprise reworked gravels of the Goldstream Formation (Péwé, 1975). The region's continental climate has a mean annual temperature of −3.3°C and monthly average temperatures of −31.7°C in January and 20.2°C in July, with absolute extremes ranging from −51°C to 38°C (Jorgenson *et al.*, 2001). The average annual wet precipitation is 407 mm and the typical average annual snowfall is 1.7 m. Permafrost is discontinuous in the region, largely confined to valley bottoms, north-facing slopes and other areas with poorly drained soils.

Permafrost exposed in the CRREL Permafrost Tunnel (Shur *et al.*, 2004) is predominantly syngenetic. The sequences preserved are dated at between ∼11 000 and ∼30 000 years BP based on radiocarbon ages and they are overlain by Holocene deposits (Sellmann, 1967; Hamilton *et al.*, 1988; Long and Péwé, 1996). The cryostructures and stratigraphy of the tunnel have been described in detail in several previous publications (Shur *et al.*, 2004; Bray *et al.*, 2006; Fortier *et al.*, 2008; Kanevskiy *et al.*, 2008).

Gravimetric moisture contents of undisturbed syngenetically frozen silt in the main tunnel adit vary from 50 per cent to 200 per cent, averaging 130 per cent (Bray *et al.*, 2006). A similar range in gravimetric moisture content (100 − 240%) is found in the winze (Kanevskiy *et al.*, 2008). The organic matter content of undisturbed syngenetically frozen silt varies from 3 per cent to 9.5 per cent while it varies from 7 per cent to 23 per cent for sediments reworked by erosive events (Hamilton *et al.*, 1988; Kanevskiy *et al.*, 2008).

WEDGE AND THERMOKARST-CAVE ICE IN THE CRREL PERMAFROST TUNNEL

Numerous syngenetic ice wedges are exposed in the CRREL Permafrost Tunnel (Figures 1 and 2A). When an ice wedge melts, either during a warming period or as a result of thermal erosion, a depression forms in the ground surface and these commonly become sinkholes (Jorgenson *et al.*, 2006). Infiltration of water into sinkholes may cause the development of a network of interconnected underground conduits and tunnels in the permafrost (Fortier *et al.*, 2007a; Figure 2B and C). This water can thermally erode both the ice wedges and the surrounding soil, resulting in slumping and changes in drainage patterns.

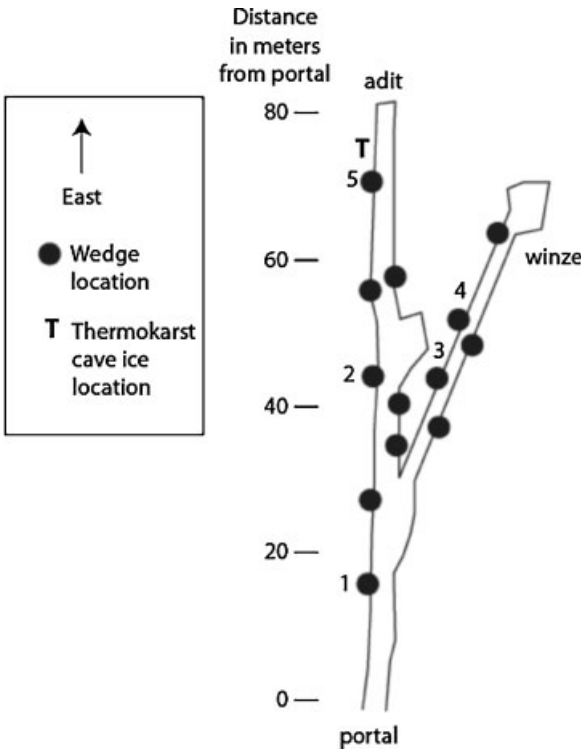

Figure 1 Overview map of the CRREL Permafrost Tunnel. The thermokarst-cave ice feature (T) and the numbered ice wedges mentioned in the text are marked.

The term 'thermokarst-cave ice' was suggested by Shumskii (1959) to describe ice features formed by the refreezing of water trapped in underground cavities, conduits and tunnels cut into the permafrost by running water (Figures 2D and 3). The geometry of thermokarst-cave ice reflects the shape of the conduits and tunnels, which often results in lenticular ice bodies with small height-to-length ratios (Shur *et al.*, 2004). Thermokarst-cave ice forms actively in areas affected by thermal erosion (slopes, areas with numerous gullies, marine coasts and riverine bluffs) and is frequently observed in the permafrost record (Fortier *et al.*, 2007b). The entry of surface water and sediment into these locations causes erosion but water and sediment can also accumulate in the pre-formed cavities. In some ice wedges within the CRREL Permafrost Tunnel, bodies of thermokarst-cave ice can be observed at several different levels within the same wedge. These bodies relate to different thermo-erosion events (in the distant past) and they may be connected by subvertical to oblique ice bodies associated with the incision of water in permafrost during the development of channels or tunnels.

Thermokarst-cave ice structures in the CRREL Permafrost Tunnel predominantly comprise lenticularly shaped, unfoliated massive ice (Shur *et al.*, 2004; Bray *et al.*, 2006). These ice bodies range from a few cm to 2 m in thickness and

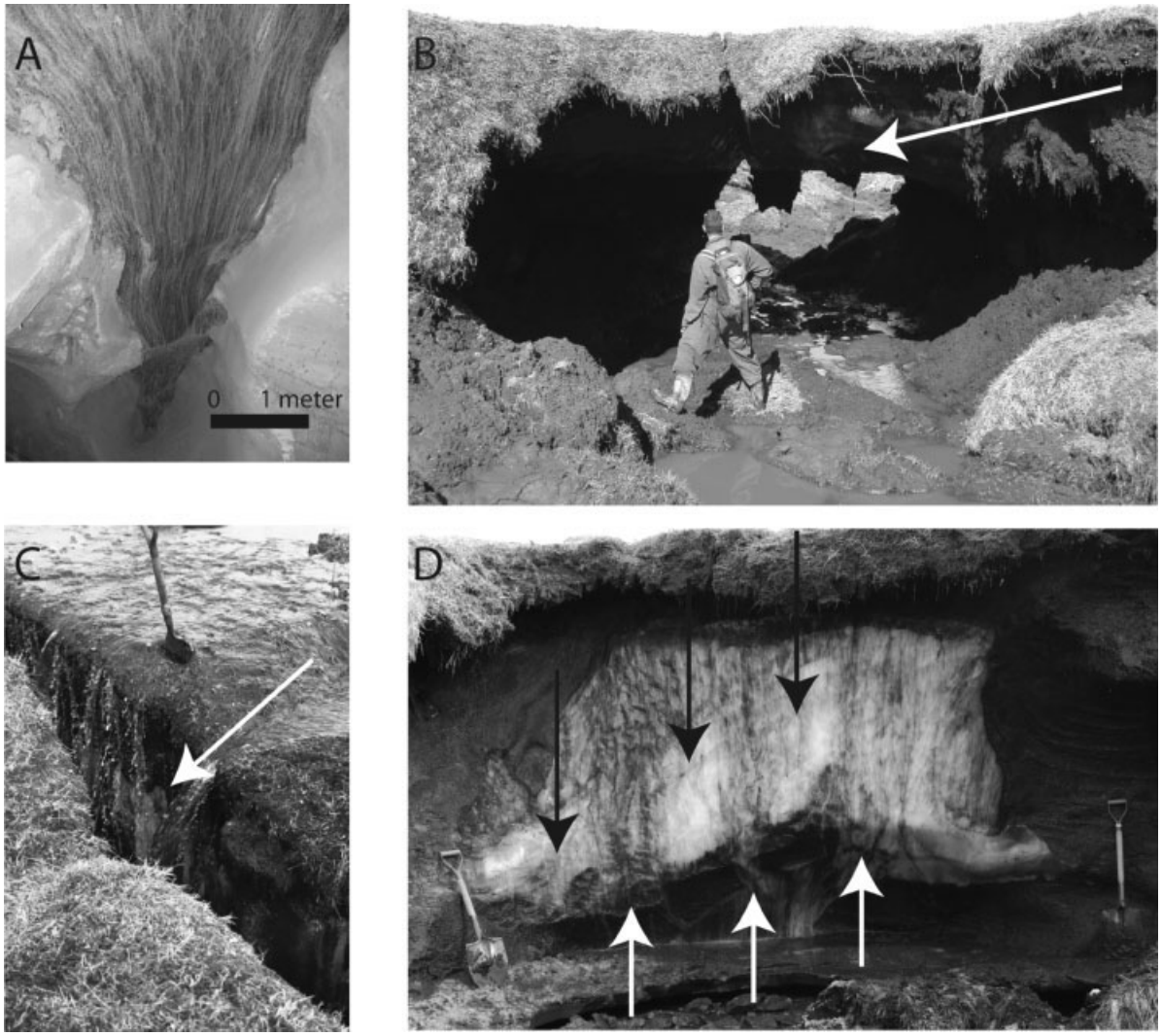

Figure 2 (A) A typical ice wedge structure in the CRREL Permafrost Tunnel. (B) Cross-section view of a tunnel formed by thermo-erosion after roof collapse, Bylot Island, Nunavut, Canada. The white arrow denotes the top of an ice wedge. (C) Surface water entering a sinkhole frost-crack enlarged by thermo-erosion in the permafrost, Bylot Island. The white arrow denotes the top of an ice wedge. (D) Thermokarst-cave ice (white, denoted by black arrows) in an ice wedge structure (ice veins were formed in the thermokarst-cave ice after its formation), Bylot Island. White arrows denote ice veins.

their greatest horizontal extent is 6 m (Shur *et al.*, 2004). This is similar to the size of active thermo-erosion tunnels observed on Bylot Island (Fortier *et al.*, 2007a). Of 20 ice wedges identified in the main CRREL tunnel adit, 19 have been subjected to thermal erosion at some time. Approximately 60 per cent of the channels cutting through the ice wedges and the surrounding syngenetic permafrost were partially or entirely filled by thermokarst-cave ice (Fortier *et al.*, 2008).

A large thermokarst-cave ice body cutting through an ice wedge is visible on the left (north) wall of the CRREL Permafrost Tunnel adit 67 to 73 m in from the tunnel portal (Bray *et al.*, 2006; Figures 1 and 3). The feature is 6 m wide and roughly 3 m tall. Bray *et al.* (2006) described the structures of the original ice wedge, thermokarst-cave ice and the surrounding soil in detail. Methane from an ice wedge located 12 m further out in the adit (wedge 5 in Figure 1) and in the same stratigraphic location yielded a radiocarbon age of 24 884 $\pm$ 139 BP (1950 AD; Katayama *et al.*, 2007). The ice wedge we investigated near the thermokarst-cave ice feature is likely about the same age.

SAMPLING AND ANALYTICAL METHODS

Core samples were collected from the upper and lower ice wedge sections surrounding the thermokarst-cave ice and from clear and cloudy lenticularly shaped thermokarst-cave ice itself (Figure 3). A 10-cm diameter by 10-cm deep hole saw was used to collect cores in triplicate from each ice feature. The outer 10-cm long core was discarded and

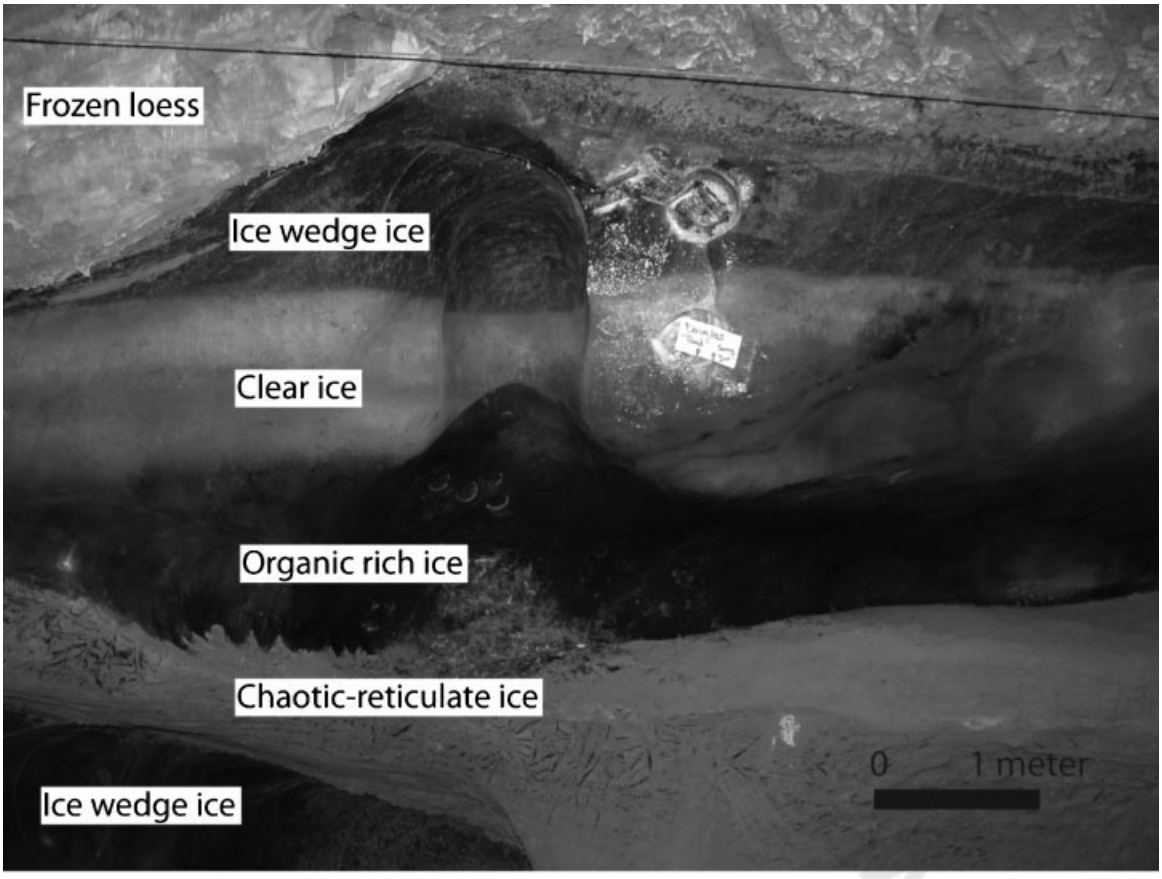

Figure 3 Photograph of the thermokarst-cave ice structure investigated in the CRREL Permafrost Tunnel. The thermokarst-cave ice body comprises clear ice and organic-rich ice. The stratified silt with chaotic-reticulate cryostructure represents the material deposited at the bottom of the underground channel after thermo-erosion of the ice wedge and is typical of inward freezing following underground thermo-erosion (Fortier *et al.*, 2008). Chaotic-reticulate ice is common in the tunnel and is caused by local (small scale) thaw modification of frozen loess. The smooth upper and lower contacts between the original ice-wedge material and the thermokarst-cave ice suggest water erosion and/or melting created the void in the ice wedge in which thermokarst-cave ice was formed.

sample cores were collected further in to exclude ice exposed to the ambient tunnel atmosphere. Each set of three sample cores was combined and melted in a pre-cleaned amber glass bottle, producing roughly 2 L of meltwater. The electrical conductivity, pH and alkalinity (by Gran titration) were measured from 60-mL subsamples. The remaining water was subsampled for biogeochemical analyses. We also collected core samples in triplicate from four ice wedges (see Figure 1) using the same coring and subsampling protocols.

Samples for major element analyses were filtered through acid-washed 0.45-μm polypropylene filters. Major cation and anion concentrations were quantified with a Dionex ICS-3000 ion chromatograph using an AS-19 anion column and a CS-12A cation column (Dionex Corporation Sunnyvale, California), each with a 10-μL injection volume. A gradient method using potassium hydroxide eluent ranged from 20 μM to 35 μM in concentration for anion analyses, while cation analyses used methane sulfonic acid eluent with a concentration of 25 μM in isocratic mode. The flow rate was 1 mL/min and the operating temperature was 30°C. The ion chromatograph was calibrated using standards with a range of values from 0.5 to 50 mg/L. Repeat analyses of calibration standards from 0.5 to 50 mg/L yielded a calculated precision for the analyses of ± 4 per cent. Peaks were identified using Chromeleon (Dionex) and verified visually.

Concentrations of dissolved organic carbon (DOC) and total dissolved nitrogen (TDN) were measured with a high-temperature combustion total organic carbon analyser (Shimadzu TOC-V) interfaced with a nitrogen detector (TNM-1, Shimadzu Corporation Kyoto, Japan; Guo and Macdonald, 2006). The total DOC blank (including Milli-Q water (Millipore Corporation Billerica, Massachusetts), acid for sample acidification and the instrument blank) was usually less than 10 μmol/L. Precision is better than 2 per cent and accuracy is within 1 per cent, on the basis of DOC standards and replicate measurements.

Stable isotopes of hydrogen and oxygen were measured using a Thermo Delta V mass spectrometer interfaced with a TC/EA pyrolysis oven (Thermo Scientific Waltham, Massachusetts) at the University of Alaska Fairbanks Alaska Stable Isotope Facility. Samples were analysed in triplicate.

Multiple analyses of standards and replicate analyses of samples yield a precision generally better than $\pm 0.4‰$ for oxygen ($\delta^{18}O$) and $\pm 2.0‰$ for hydrogen isotopes (δD). Data are reported in reference to VSMOW-SLAP-GISP calibration.

RESULTS AND DISCUSSION

Biogeochemical and Physical Characteristics of Thermokarst-Cave and Wedge Ice

The biogeochemical results from our analyses are summarised in Table 1. For comparison, we have also included the maximum and minimum values for each biogeochemical parameter measured in the Chena River (Cai *et al.*, 2008a, 2008b) which drains a 5200-km^2 boreal-forested watershed in discontinuous permafrost and flows within 12 km of the CRREL Permafrost Tunnel. These values provide a reference for surface water chemistry in the region.

The upper and lower ice wedge sections in the thermokarst-cave ice structure and the other four reference ice wedges have similar biogeochemical characteristics. Reference ice wedge 1 has a higher pH and alkalinity but a similar biochemical signature (DOC and TDN) to the other three reference ice wedges and the ice wedge bodies above and below the thermokarst-cave ice. The ice wedges yield major element concentrations within an order of magnitude of the Chena River values and contain slightly more DOC and TDN than the highest concentrations measured in the Chena River.

Table 1 A summary of the biogeochemical measurements of the thermokarst-cave ice bodies and surrounding ice wedge and reference ice wedges in the CRREL Permafrost Tunnel. Reference ice wedges 1 and 2 are located 43 m and 19 m in from the main adit on the left wall of the tunnel, respectively (Bray *et al.*, 2006). Reference ice wedges 3 and 4 are located 25 m and 18 m in from the back of the winze on the left wall of the tunnel, respectively (Kanevskiy *et al.*, 2008). Maximum and minimum values for each biogeochemical constituent measured during a one-year study of the Chena River (Cai *et al.*, 2008b; T. A. Douglas, unpublished data) are also included.

Ice feature	Upper ice wedge	Upper thermokarst-cave ice	Lower thermokarst-cave ice	Lower ice wedge	Reference ice wedge 1	Reference ice wedge 2	Reference ice wedge 3	Reference ice wedge 4	Chena River minimum to maximum
Specific conductance (μS/cm)	117	54	3340	110	455	81	175	87	117 to 237[1]
pH	7.46	6.73	8.97	7.87	9.02	7.43	7.33	7.39	6.9 to 7.9[1]
Sodium (mg/L)	1.6	1.2	7.4	1.5	1.5	1.0	1.3	1.0	1.6 to 3.9[2]
Potassium (mg/L)	9.1	1.3	240.1	10.6	9.1	4.4	18.2	7.1	0.9 to 2.4[2]
Magnesium (mg/L)	0.4	0.2	19.7	0.5	2.6	0.5	0.7	0.4	1.0 to 2.4[2]
Calcium (mg/L)	1.0	0.5	96.7	1.4	10.7	1.2	1.1	0.9	15.1 to 31.4[2]
Alkalinity (mg/L)[3]	26.8	6.4	1098.2	39.0	153.3	29.1	81.5	44.6	38.4 to 88.5[1]
Fluoride (mg/L)	0.1	0.3	0.6	0.3	0.1	0.1	0.7	0.1	0.1 to 0.2[2]
Chloride (mg/L)	3.5	2.4	7.0	5.5	1.0	3.2	8.5	3.3	0.5 to 1.9[2]
Nitrate (mg/L)	0.1	0.5	4.33	0.2	0.2	0.1	0.2	0.2	0.5 to 1.5[2]
Sulfate (mg/L)	5.4	3.1	1385	6.9	18.2	4.0	8.3	4.1	17.7 to 24.3[2]
Dissolved organic carbon (mg/L)	21.1	8.7	613.6	21.8	20.5	18.4	68.5	22.2	2.5 to 14.2[1]
Total dissolved nitrogen (mg/L)	3.9	1.3	73.2	3.8	4.6	3.8	9.4	3.9	0.2 to 0.7[1]
$\delta^{18}O$ (‰)	-25.3	−24.4	−27.0	−26.1	−29.3	−25.4	−26.5	−24.1	−23.1 to −19.4[2]
δD (‰)	−200.5	−191.3	−210.4	−204.4	−219.8	−199.7	−206.3	−193.0	−163.4 to −147.9[2]

[1] Chena River data from Cai *et al.* (2008b).
[2] Chena River data from T. A. Douglas (unpublished data).
[3] Alkalinity measured by Gran titration.

The lenticularly shaped thermokarst-cave ice has an upper clear ice facies and a lower cloudy to brownish-orange ice facies (Figure 3). These two ice sub-layers yield markedly different biogeochemical characteristics from one another, wedge ice surrounding the thermokarst-cave ice and the four reference ice wedges. The upper (clear) ice contains extremely low major element concentrations compared with all the other ice collected in the tunnel and the range of values reported for the Chena River. It contains DOC and TDN concentrations that are roughly half that of the upper and lower ice wedge samples and the four reference ice wedge samples. The DOC and TDN concentrations measured in the upper ice wedge are at the high end of the Chena River water samples.

The lower (cloudy) sub-layer of thermokarst-cave ice yields major element, DOC and TDN values that are far greater than any other ice body in the CRREL Permafrost Tunnel and are 10 to 100 times greater than the highest biogeochemical load in the Chena River. Of particular note are the elevated alkalinity, potassium, and sulfate concentrations in the lower ice compared with the other ice bodies in the tunnel. The lower sub-layer of thermokarst-cave ice, which is visibly dark brown in colour, is underlain by sandy silts with a well-developed reticulate-chaotic cryostructure (Figure 3).

The stable oxygen isotope values of wedge and thermokarst-cave ice in the CRREL Permafrost Tunnel range between −29.3 and −24.1 ‰. These values are slightly lower than the minimum values measured in the Chena River. As a comparison, biweekly samples of the Chena River collected for one year yielded $\delta^{18}O$ values of −23.1 to −19.4 ‰ (n = 26, mean = −21.4‰; T. A. Douglas, unpublished data). Stable hydrogen isotope values from ice wedge material are also similar to one another and slightly lower than the most deuterium-depleted values from the Chena River. Stable oxygen and hydrogen isotope values for the clear and cloudy thermokarst-cave ice material are within the range of values from the four ice-wedge samples. The $\delta^{18}O$ and δD values of the clear and cloudy thermokarst-cave ice material are slightly lower than the most isotopically depleted Chena River values.

Formation of Thermokarst-Cave Ice

The sequence of events that likely formed and preserved the thermokarst-cave ice feature is shown in Figure 4, but the amount of time associated with each step is largely speculative. In the Late Pleistocene, active deposition of loess, reworking of loess and deposition of other sedimentary material laid down material comprising the Goldstream Formation (Péwé, 1975). Ice wedges developed in the area contemporaneously with sedimentation and syngenetic permafrost formation (Figure 4, step 1; Shur *et al.*, 2004).

Thermokarst development and the subsequent infiltration of surface runoff into the permafrost through a sinkhole or other depression in the ground surface cut a channel horizontally through the ice wedge material and some of the surrounding loess and gravels, creating a cavity roughly 1 m high and 6 m wide (Figure 4, steps 2 and 3). This could have occurred within a matter of one summer due to the potential erosive power of surface water and the susceptibility of ice wedges to erosion, as has been observed on Bylot Island (Figure 2B − D; Fortier *et al.*, 2007a). Surface waters filled the thermo-erosional cavities, and soil and plant material brought in by the water settled to the bottom (Figure 3 and Figure 4, step 4). The wedge remained intact above and below the thermokarst-cave ice (i.e. it does not exhibit signs of slumping or shifting), which indicates that the underground channels were cut into frozen material. Water trapped in the tunnel was likely submitted to inward freezing from the underground channel walls to create the thermokarst-cave ice body that has remained frozen since.

The present colour, structure and geochemical characteristics of the thermokarst-cave ice located between the upper and lower portions of the ice wedge suggest the waters contained organic-rich material. The water likely froze top-down, with the clear (upper) body of lenticularly shaped ice freezing prior to the cloudy (lower) ice. These layers likely formed through exclusion of solutes during ice formation from the upper layer to the lower layer (e.g. Belzile *et al.*, 2002). This is supported by the lower concentrations of major element and biogeochemical constituents in the clear ice and the highest $\delta^{18}O$ and δD values of any of the ice present in the ice wedge replacement structure. This process was likely similar to stable isotope (and major element and organic compound) fractionation that occurs during ice formation on lakes and rivers, which leads to the enrichment of heavy isotopes in the condensed phase (ice) (e.g. Hoefs, 2004). Inorganic and organic solutes are excluded from new ice in the same manner. The greater stable isotope values in the clear, upper lenticular massive ice are indicative of the initial onset freezing of water. The lower, dark layer of massive ice contains far greater concentrations of major element and biochemical constituents and is attributed to freezing of the remaining organic-rich waters at the base of the underground channel.

Loess and sedimentary material associated with further syngenetic permafrost aggradation continued to be deposited on the surface above the thermokarst-cave ice structure (Figure 4, step 5). It is now located roughly 20 m below the ground surface (Sellman, 1967). In many cases, growth of ice wedges continued after the formation of a thermokarst-cave ice body. Such ice bodies crossed by ice veins or wedges can be observed both in the main adit and the winze (Figure 2D; Shur *et al.*, 2004, Figure 4).

High concentrations of DOC and other solutes inside the CRREL Permafrost Tunnel revealed here have important implications. First, they will lead to an improved estimate of DOC and solutes exported from permafrost should permafrost thaw during climate warming. In the CRREL Permafrost Tunnel the thermokarst-cave ice has orders of magnitude greater nutrient concentrations than ice wedge ice nearby. This suggests that approximations of the nutrient content in permafrost may be underestimated in locations where secondary ice wedge material has been replaced by thermokarst-cave ice. Second, our results show that the

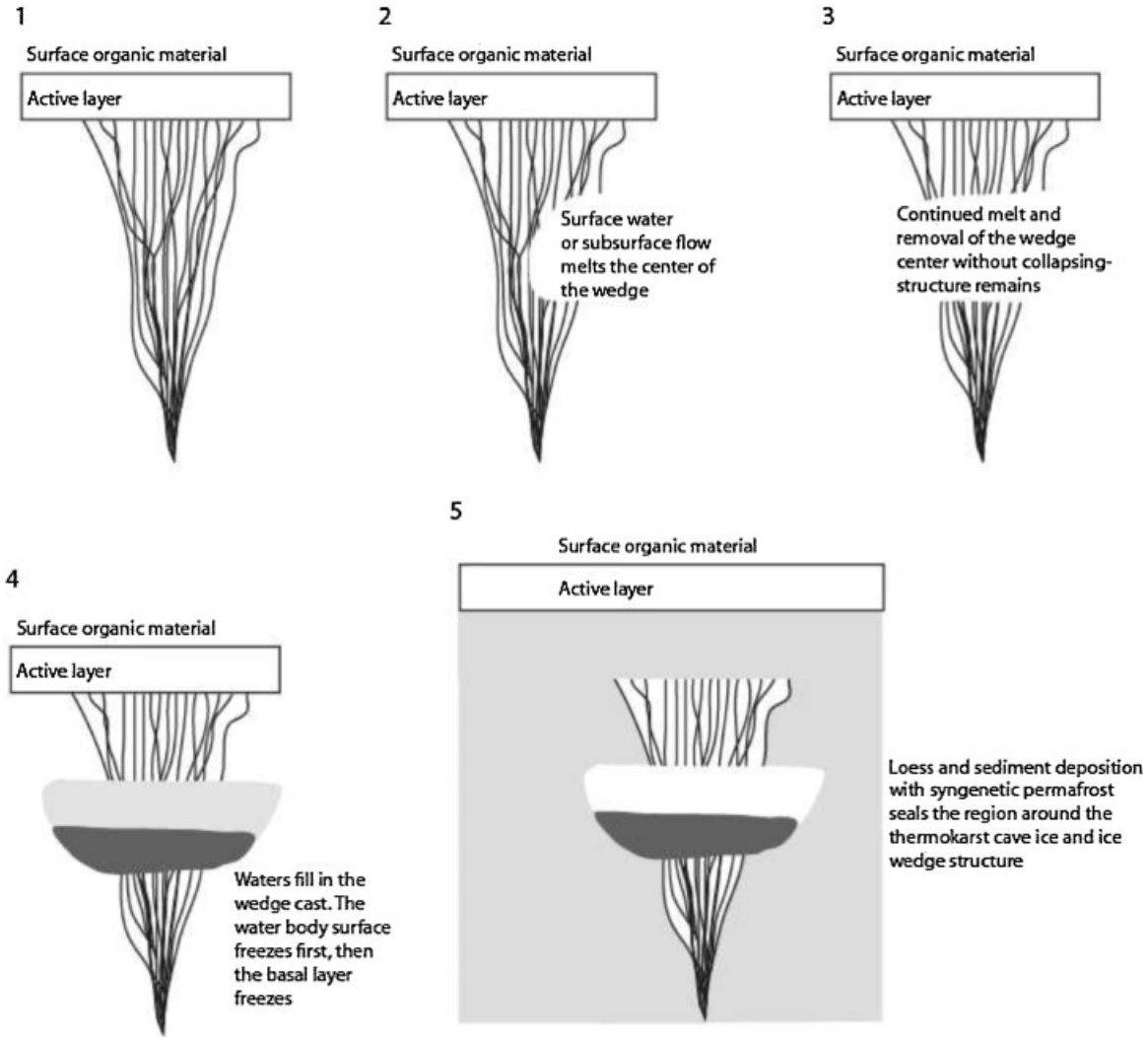

Figure 4 Schematic diagram of the processes that formed and preserved the thermokarst-cave ice feature investigated in the CRREL Permafrost Tunnel.

DOC and solute contents of ice are not always lower than typical river water-draining permafrost landscapes. Third, DOC and other organic materials preserved in permafrost (including thermokarst-cave ice) could participate in surface biogeochemical cycling if they are released due to permafrost degradation.

CONCLUSIONS

The results of our study suggest that thermokarst-cave ice contains markedly higher nutrient and major element concentrations than primary ice wedge ice nearby. The thermokarst-cave ice yields major element and biochemical concentrations that are 29 (DOC), 19 (TDN), 72 (nitrate), 256 (sulfate) and 26 (potassium) times greater than those measured in the ice wedge material surrounding the studied massive thermokarst-cave ice or four other ice wedges investigated in the CRREL Permafrost Tunnel. Although we cannot estimate the prevalence or spatial extent of thermokarst-cave ice in other permafrost conditions or locales, our results suggest that biogeochemical characteristics of these features should be incorporated into estimates of the amount of carbon stored in permafrost regions.

ACKNOWLEDGEMENTS

The constructive comments of Hugh French, three reviewers and the Editor Antoni Lewkowicz greatly strengthened the manuscript. This project was funded by the National Science Foundation Office of Polar Programs (#0454939).

REFERENCES

Allard M, Kasper JN. 1998. Temperature conditions for ice wedge cracking: Field measurements from Salluit, northern

Québec. In *Permafrost, Seventh International Conference*, Lewkowicz AG, Allard M (eds). Université Laval: Québec; Nordicana 57: 5–12.

Belzile CJ, Gibson AE, Vincent WF. 2002. CDOM and DOC exclusion from lake ice: Implications for irradiance transmission and carbon cycling. *Limnology and Oceanography* **45**: 1283–1293.

Bockheim JG, Hinkel KM. 2007. The Importance of 'Deep' Organic Carbon in Permafrost-Affected Soils of Arctic Alaska. *Soil Science Society of America Journal* **71**: 1889–1892.

Bray MT, French HM, Shur Y. 2006. Further cryostratigraphic observations in the CRREL Permafrost Tunnel, Fox, Alaska. *Permafrost and Periglacial Processes* **17**(3): 233–243. DOI: 10.1002/ppp.558

Burn CR. 1998. The response (1958-1997) of permafrost and near-surface ground temperatures to forest fire, Takhini River valley, southern Yukon Territory. *Canadian Journal of Earth Science* **35**: 184–199.

Cai Y, Guo L, Douglas TA, Whitledge TE. 2008a. Seasonal variations in nutrient concentrations and speciation in the Chena River, Alaska. *Journal of Geophysical Research Biogeosciences* **113**: G03035. DOI: 10.1029/2008JG000733

Cai Y, Guo L, Douglas TA. 2008b. Temporal variations in organic carbon species and fluxes from the Chena River, Alaska. *Limnology and Oceanography* **53**(4): 1408–1419.

Douglas TA, Jorgenson MT, Kanevskiy MZ, Romanovsky VE, Shur Y, Yoshikawa K. 2008. Permafrost dynamics at the Fairbanks Permafrost Experimental Station near Fairbanks, Alaska. In *Proceedings of the Ninth International Conference on Permafrost*, Kane DL, Hinkel KM (eds). Institute of Northern Engineering University of Alaska Fairbanks: Fairbanks, Alaska; 373–378.

Fortier D, Allard M, Shur Y. 2007a. Observation of rapid drainage system development by thermal erosion of ice wedges on Bylot Island, Canadian Arctic Archipelago. *Permafrost and Periglacial Processes* **18**(3): 229–243. DOI: 10.1002/ppp.595

Fortier D, Kanevskiy MZ, Shur Y. 2007b. Ground ice formed after thermoerosion of the permafrost in Alaska. *EOS, Transactions of the American Geophysical Union* **88**(52): Fall Meeting Supplement, abstract C21A-0060.

Fortier D, Kanevskiy MZ, Shur Y. 2008. Genesis of reticulate-chaotic cryostructure in permafrost. In *Proceedings of the Ninth International Conference on Permafrost*, Kane DL, Hinkel KM (eds). Institute of Northern Engineering University of Alaska Fairbanks: Fairbanks, Alaska; 451–456.

French HM. 1975. Pingo investigations and terrain disturbance studies, Banks Island, District of Franklin. In Current Research, Part A, Geological Survey of Canada, Paper 75-1A, 459–464.

Gasanov SS. 1969. *Structure and History of Formation of Permafrost in Eastern Chukotka*. Nauka: Moscow; 168pp (in Russian).

Guo L, Macdonald RW. 2006. Sources and transport of terrigenous organic matter in the upper Yukon River: Evidence from isotope (^{13}C, ^{14}C and ^{15}N) composition of dissolved, colloidal and particulate phases. *Global Biogeochemical Cycles* **20**: GB2011.

Guo L, Ping C-L, Macdonald RW. 2007. Mobilization pathways of organic carbon from permafrost to arctic rivers in a changing climate. *Geophysical Research Letters* **34**: L13603.

Hamilton TD, Craig JL, Sellmann PV. 1988. The Fox permafrost tunnel: A late Quaternary geologic record in central Alaska. *Geological Society of America Bulletin* **100**(6): 948–969.

Hinzman LD, Fukuda M, Sandberg DV, Chapin FS III, Dash D. 2003. FROSTFIRE: An experimental approach to predicting the climate feedbacks from the changing boreal fire regime. *Journal of Geophysical Research* **108**(D1): 8153.

Hoefs J. 2004. *Stable Isotope Geochemistry.* Springer: Berlin; 340pp.

Jorgenson MT, Racine CH, Walters JC, Osterkamp TE. 2001. Permafrost degradation and ecological changes associated with a warming climate in central Alaska. *Climatic Change* **48**: 551–579.

Jorgenson MT, Shur YL, Pullman ER. 2006. Abrupt increases in permafrost degradation in Arctic Alaska. *Geophysical Research Letters* **33**: L02503.

Kanevskiy MZ, Fortier D, Shur Y, Bray M, Jorgenson MT. 2008. Detailed cryostratigraphic studies of syngenetic permafrost in the winze of the CRREL Permafrost Tunnel, Fox, Alaska. In *Proceedings of the Ninth International Conference on Permafrost*, Kane DL, Hinkel KM (eds). Institute of Northern Engineering University of Alaska Fairbanks: Fairbanks, Alaska; 889–894.

Katayama T, Tanaka M, Moriizumi J, Nakamura T, Brouchkov A, Douglas TA, Fukuda M, Tomita F, Asano K. 2007. Phylogenetic Analysis of Bacteria Preserved in a Permafrost Ice Wedge for 25,000 Years. *Applied and Environmental Microbiology* **73**(7): 2360–2363.

Linell KA. 1973. Long-term effects of vegetative cover on permafrost stability in an area of discontinuous permafrost. In *Proceedings of Permafrost: North American Contribution to the Second International Conference*. National Academy of Sciences, National Research Council: Washington, D.C., USA, 688–693.

Long A, Péwé TL. 1996. Radiocarbon dating by high-sensitivity liquid scintillation counting of wood from the Fox Permafrost Tunnel near Fairbanks, Alaska. *Permafrost and Periglacial Processes* **7**(3): 281–285.

Mackay JR. 1997. A full scale field experiment (1978-1995) on the growth of permafrost by means of lake drainage, western Arctic coast: a discussion of the method and some results. *Canadian Journal of Earth Sciences* **34**: 17–34.

Murton JB, French HM. 1993. Thaw modification of frost-fissure wedges, Richards Island, Pleistocene Mackenzie Delta, Western Arctic Canada. *Journal of Quaternary Science.* **8**(3): 185–196.

Oechel WC, Hastings SJ, Vourlitis G, Jenkins M, Reiechers G, Grulke N. 1993. Recent change of Arctic tundra ecosystems from a net carbon dioxide sink to a source. *Nature* **361**: 520–523.

Petrone KC, Jones JB, Hinzman LD, Boone RD. 2006. Seasonal export of carbon, nitrogen, and major solutes from Alaskan catchments with discontinuous permafrost. *Journal of Geophysical Research* **111**: G02020.

Péwé TL. 1975. Quaternary geology of Alaska. United States Geological Survey Professional Paper 835; 145pp.

Popov AI, Rozenbaum GE, Tumel NV. 1985. *Cryolithology.* Moscow University Press: Moscow; 239pp (in Russian).

Rozenbaum GE, Arkhangelov AA, Konyakhin MA. 1978. Thermokarst-cave ice of the Yana-Kolyma lowland. *Problems of Cryolithology* **VII**: 74–92 (in Russian).

Sellmann PV. 1967. Geology of the USACRREL Permafrost Tunnel, Fairbanks, Alaska. US Army Cold Regions Research and Engineering Laboratory Technical Report 199, Hanover, New Hampshire; 22pp.

Shumskii PA. 1964. *Chapter IX. Ground (subsurface) ice. In Principles of Geocryology (Permafrost Studies)*, Academy of Sciences of the USSR, Shvetsov PF, Dostovalov BN (eds). 1959. V.A. Obruchev Institute of Permafrost Studies: Moscow:274–327 (in Russian). National Research Council of Canada, Ottawa, Technical Translation 1130; 118pp.).

Shur Y, French HM, Bray MT, Anderson DA. 2004. Syngenetic permafrost growth: cryostratigraphic observations from the CRREL tunnel near Fairbanks, Alaska. *Permafrost and Periglacial Processes* **15**(4): 339–347. DOI: 10.1002/ppp.486

Shur YL, Jorgenson MT. 2007. Patterns of permafrost formation and degradation in relation to climate and ecosystems. *Permafrost and Periglacial Processes* **18**: 7–19. DOI: 10.1002/ppp.582

Tarnocai C, Canadell JG, Schuur EAG, Kuhry P, Mazhitova G, Zimov S. 2009. Soil organic carbon pools in the northern circumpolar permafrost. *Global Biogeochemical Cycles* **23**: GB2023. DOI: 10.1029/2008GB003327.

Viereck LA. 1982. Effects of fire and firelines on active layer thickness and soil temperatures in interior Alaska. In *Proceedings of the Fourth Canadian Permafrost Conference*. National Research Council of Canada Calgary: Ottawa, Ontario; 123–135.

Vtyurin BI. 1964. *Cryogenic structure of Quaternary deposits*. Nauka: Moscow; 151pp (in Russian).

Zimov SA, Schuur EAG, Chapin FS III. 2006a. Permafrost and the global carbon budget. *Science* **312**: 1612–1613.

Zimov SA, Davydov SP, Zimova GM, Davydova AI, Schuur EAG, Dutta K, Chapin FS III. 2006b. Permafrost carbon: Stock and decomposability of a globally significant carbon pool. *Geophysical Research Letters* **33**: L20502. DOI: 10.1029/2006GL027484.